Research Square

Preprints are preliminary reports that have not undergone peer review.
They should not be considered conclusive, used to inform clinical practice,
or referenced by the media as validated information.

Machine Learning–Guided QSAR Screening of Fluconazole Analogs and FDA-Approved Drugs against Candida albicans, with Docking, Molecular Dynamics, and ADMET Analysis

Hamza Age Daudo

tarmamadehamzaagedaudo@gmail.com

Lúrio University

Emmanuel Silva Marinho

State University of Ceará

Victor Moreira de Oliveira

State University of Ceará

Márcia Machado Marinho

State University of Ceará

Ribeiro Vasco Ribeiro

Lúrio University

Research Article

Keywords: Candida albicans, machine learning, QSAR, molecular docking, molecular dynamics, ADMET

Posted Date: March 30th, 2026

DOI: https://doi.org/10.21203/rs.3.rs-9212005/v1

License: This work is licensed under a Creative Commons Attribution 4.0 International License.
Read Full License

Additional Declarations: No competing interests reported.

Version of Record: A version of this preprint was published at Molecular Diversity on August 7th, 2026.
See the published version at https://doi.org/10.1007/s11030-026-11621-3.

Machine Learning–Guided QSAR Screening of Fluconazole Analogs and FDA-Approved Drugs against *Candida albicans*, with Docking, Molecular Dynamics, and ADMET Analysis

1. Hamza Age Daudo, Pharmacist, Lúrio University, Mozambique, Email: tarmamadehamzaagedaudo@gmail.com, Orcid https://orcid.org/0009-0003-2664-8550 *
2. Emmanuel Silva Marinho, Postgraduate Program in Natural Sciences, State University of Ceará, Fortaleza, CE, Brazil[1]; Postgraduate Program in Veterinary Sciences, State University of Ceará, Fortaleza, CE, Brazil[2]; Chemistry Course, Science and Technology Center, State University of Ceará, Fortaleza, CE, Brazil[3], Email emmanuel.marinho@uece.br, ORCID https://orcid.org/0000-0002-4774-8775
3. Victor Moreira de Oliveira, Laboratory of Bioprospecting and Monitoring of Natural Resources (LBMRN), State University of Ceará (UECE), Fortaleza, CE, 60714-903, Brazil; Doctoral Program in Biotechnology (RENORBIO); Master's Program in Natural Sciences (PPGCN), Email: vitor.moreira@aluno.uece.br, Orcid: https://orcid.org/0000-0002-9261-5656
4. Márcia Machado Marinho, Postgraduate Program in Natural Sciences, State University of Ceará (UECE), Fortaleza, CE, Brazil, Email marcia.marinho@uece.br, ORCID https://orcid.org/0000-0002-7640-2220
5. Ribeiro Vasco Ribeiro, Lúrio University, Mozambique, Email: rribeiro@unilurio.ac.mz, ORCID: https://orcid.org/0000-0002-3898-1735

* Corresponding Author:

ABSTRACT

Fungal infections are a growing public health concern, particularly those caused by *C. albicans*, which has been classified by the WHO as a critical-priority pathogen. The limited treatment options and increasing fluconazole resistance highlight the need for novel antifungal agents. This study employed a machine learning-guided QSAR workflow as the main strategy to identify fluconazole analogs and FDA-approved drugs with potential activity against *C. albicans*, with molecular docking, molecular dynamics, and ADMET analyses used as complementary post-screening tools. Regression-based ML models (Extra Trees, Gradient Boosting, and Random Forest) were trained on curated ChEMBL bioactivity data to predict antifungal potency and prioritize candidates, with no significant performance differences among the models (Friedman test, $p = 0.061$). ML-driven virtual screening identified ZINC000299869730 as the top candidate. Docking against *exo-(1,3)-glucanase* (PDB ID: 1EQP) predicted a higher *in silico* binding affinity (–10.27 kcal/mol) than fluconazole (–8.87 kcal/mol), suggesting a potentially stronger interaction. Additional docking against CYP51 indicated a possible multitarget profile. Molecular dynamics simulations over 200 ns indicated intermediate complex stability with moderate local flexibility, whereas ADMET predictions suggested a pharmacokinetic and safety profile comparable to that of fluconazole. Overall, this study highlights the central role of QSAR/ML models in candidate prioritization and demonstrates how molecular docking and molecular dynamics complement ML predictions, positioning ZINC000299869730 as a computationally prioritized antifungal lead and supporting ML-guided pipelines for antifungal lead identification.

Keywords: *Candida albicans*, machine learning, QSAR, molecular docking, molecular dynamics, ADMET.

1 INTRODUCTION

Fungal infections pose a growing threat to global public health, notably those caused by *Candida albicans*, classified by the World Health Organization (WHO) as a critical-priority fungal pathogen, alongside *Cryptococcus neoformans*, *Candida auris*, and *Aspergillus fumigatus* [1]. These infections affect over 6.5 million people annually, resulting in approximately 3.7 million deaths per year [1,2].

Among fungal infections, invasive candidiasis holds a prominent position, with over 1.5 million annual cases and mortality rates reaching 50%–60% in immunocompromised patients [3]. Candidemia, the main manifestation of invasive candidiasis, is predominant in hospital settings and accounts for over 85% of all fungemia cases in Europe and the United States [3]. Furthermore, vulvovaginal candidiasis (VVC) affects up to 75% of women at some point in their lives, and up to 10% may experience recurrent episodes (RVVC), highlighting its high prevalence and clinical impact [3,4].

The current antifungal therapeutic arsenal is limited in terms of the number of available classes and efficacy against increasing resistance rates. Fluconazole, an azole widely used in the treatment of candidiasis, especially in uncomplicated forms and as "step-down" therapy for invasive candidiasis, has shown increasing resistance rates, particularly in *C. auris* (>90%), *C. tropicalis* (1–20%), and *C. albicans* [5–7]. Studies have demonstrated that approximately 23% of *C. albicans* clinical isolates obtained from vaginal cultures exhibit fluconazole resistance, with an upward trend in recent years [5].

Given this scenario, the need for novel antifungal agents is evident. The identification and prioritization of potential candidates is a strategic and multifaceted process that traditionally involves screening large chemical libraries, biological evaluation, and structural optimization of lead compounds. However, these approaches are often costly, time-consuming, and have low success rates [8].

In this context, the integration of Artificial Intelligence (AI)-based tools has revolutionized pharmaceutical research by enabling the efficient analysis of large data volumes and the identification of complex structural patterns undetectable by conventional methods [9]. Machine Learning (ML) approaches are being widely employed to predict bioactivity properties, structure-activity relationships, and toxicity, optimizing the selection and prioritization of candidate compounds with greater speed and accuracy [10,11].

Building on this paradigm, the present study employed an ML-guided Quantitative Structure–Activity Relationship (QSAR) workflow as the central strategy to identify structural analogs of fluconazole and FDA-approved drugs with potential antifungal activity against *C. albicans*. Molecular docking, molecular dynamics (MD) simulations, and Absorption, Distribution, Metabolism, Excretion, and Toxicity (ADMET) analyses were used as complementary tools for post-screening evaluation.

2 MATERIALS AND METHODS

2.1 STUDY FLOWCHART

The present study followed the workflow illustrated in Figure 1, in which the compound selection was primarily guided by chemometric analysis using ML models. The steps were as follows: (i) collection of bioactivity data against *Candida albicans* from the ChEMBL database; (ii) data pre-processing, including cleaning, standardization, and normalization; (iii) generation of molecular descriptors using Morgan fingerprints; (iv) exploratory dimensionality reduction using Principal Component Analysis (PCA); (v) feature selection to identify the most relevant descriptors; (vi) benchmarking of 42 regression algorithms using the Lazy Predict framework; (vii) selection of the three best-performing models based on predictive performance; (viii) hyperparameter optimization and cross-validation of the selected models; (ix) virtual screening of compounds from the ZINC-22 database and FDA-approved drugs to validate the models and explore drug repositioning opportunities; (x) statistical analysis of screened compounds based on predicted pIC_{50} values and consensus evaluation across the ML models, defining the primary candidates; (xi) structural similarity analysis between the screened ZINC-22 compounds and fluconazole; (xii) molecular docking simulations against the target enzyme using fluconazole as a reference; (xiii) MD simulations of the best-ranked protein–ligand complexes; and (xiv) *in silico* evaluation of ADMET properties of the selected candidates [12].

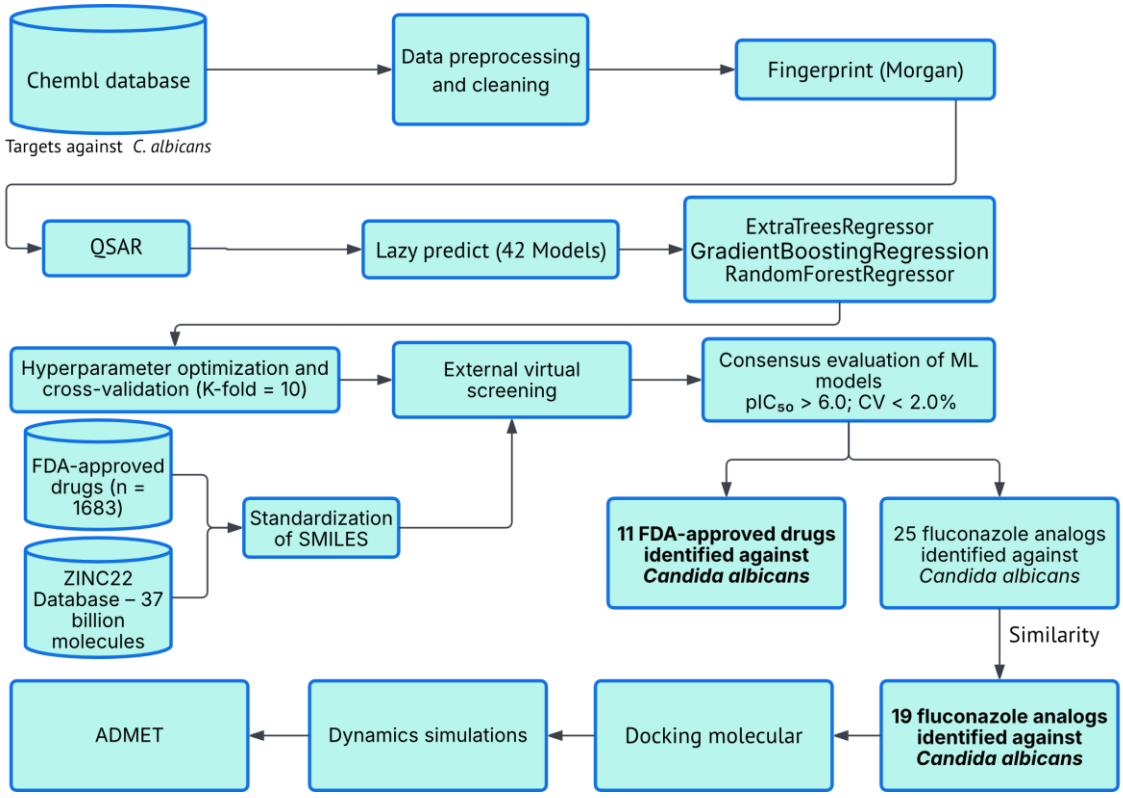


Figure 1. Flowchart detailing the integrated computational approach used for data collection and cleaning, training and validation of ML models, molecular docking, and MD simulations. The workflow aims to predict new drug candidates from ZINC-22 (Fluconazole analogs) and identify repurposed FDA-approved drugs effective against *C. albicans.*

2.2 DESCRIPTION OF THE CHEMBL DATABASE

The data used in this study for the development of ML models aimed at predicting the bioactivity of compounds against *C. albicans* were obtained from the ChEMBL database [13]. ChEMBL is a resource provided by the European Bioinformatics Institute that contains detailed bioactivity information on more than 2.5 million compounds with pharmacological properties [13]. This database integrates chemical and bioactivity information, facilitating drug discovery [14].

2.2.1 Description of the Dataset Used

The dataset employed in this study comprised 81,714 bioactivity records corresponding to 40,790 compounds associated with the target CHEMBL366 [15]. The retrieved data included multiple bioactivity endpoints, such as half-maximal effective concentration (EC_{50}), minimum inhibitory concentration (MIC), inhibition constant (K_i), activity and inhibition percentages, and half-maximal inhibitory concentration (IC_{50}). For model development, only IC_{50} measurements were retained, given their widespread adoption in QSAR studies and direct representation of compound potency [16]. IC_{50} values (expressed in molar units) were converted to pIC_{50} using a logarithmic transformation ($pIC_{50} = -\log_{10} IC_{50}$), which enabled a more suitable scale for comparative analyses [16]. Data curation and preprocessing involved the selection of functional (F-type) assays, accounting for > 95% of the records [17]. Additional steps included replacing infinite values with null entries, removing records containing missing values (NaN), and excluding compounds lacking valid bioactivity measurements or structural representations [18].

2.3 CALCULATION OF MORGAN FINGERPRINT DESCRIPTORS

The molecular fingerprint descriptors were calculated using the RDKit library by generating Morgan descriptors of the extended connectivity fingerprint type, radius 2 (ECFP4), with 2048-bit binary vectors [19]. Before descriptor generation, the molecular structures were standardized by removing salts, normalizing functional groups, neutralizing formal charges, and canonicalizing tautomers, followed by final molecule sanitization [20]. To reduce the bias and complexity of the ML models developed, a variance filter (variance < 0.01) was applied to remove descriptors with low variability from the dataset [21].

2.4 DEVELOPMENT OF MACHINE LEARNING MODELS

The data were normalized using the *StandardScaler* and subjected to PCA exclusively for exploratory analysis and preliminary benchmarking using the LazyPredict framework. PCA was applied to investigate descriptor redundancy and support the comparative evaluation of regression algorithms, facilitating the identification of the three best-performing models (Supplementary Figure S01) [22,23]. The PCA-transformed features were not used in the final model training or optimization stages; all predictive models were developed using the original molecular representations, namely binary Morgan fingerprints. The dataset was divided into training (70%) and testing (30%) subsets for the models. We employed LazyPredict as an automated screening tool to benchmark 42 regression algorithms and select the top three models based on coefficient of determination (R^2) (Supplementary Figure S02) [24]. Based on this screening, extra trees, gradient boosting, and random forest regressors were selected for the analysis. Morgan fingerprint descriptors were used as input variables, and pIC_{50} values served as the response variable [25]. The model performance was evaluated using multiple metrics, including the R^2, mean squared error (MSE), root mean squared error (RMSE), and mean absolute error (MAE) [26].

Hyperparameter optimization was performed using the Optuna framework with 100 guided search iterations based on the Tree-structured Parzen Estimator algorithm [27]. Hyperparameter configurations were assessed via 10-fold cross-validation, and the mean R^2 across the folds was used as the optimization criterion. The optimal parameter set was subsequently used to train the final models [28].

To compare the performance of the ML models, 10-fold cross-validation was performed using RMSE as the performance metric. Global differences between the models were assessed using the non-parametric Friedman test, followed by the Nemenyi post-hoc test for pairwise comparisons between models [29].

2.5 EXTERNAL VIRTUAL SCREENING

2.5.1 SMILES Standardization

Before generating molecular descriptors for external screening, SMILES were standardized using a systematic RDKit-based protocol. Invalid compounds were filtered using the following criteria: absence of carbon atoms, presence of metals or non-allowed elements (except C, H, N, O, P, S, F, Cl, Br, I), molecular weight above 1500 Da, and presence of more than five carbon-containing fragments, indicating potential mixtures. Valid compounds then underwent an iterative standardization procedure, including conversion to InChI and back to SMILES, sanitization, removal of disconnected fragments (keeping the largest), charge neutralization, removal of isotopes, stereochemistry, charge states, and tautomer standardization. The process was repeated for up to five cycles or until the SMILES were stable. When multiple standardized forms were produced, the most recurrent one was selected. The final SMILES generated through this process were used to compute molecular descriptors [20].

2.5.2 Virtual Screening

Virtual screening was performed using compounds from the ZINC-22 database, which contains more than 37 billion molecules and is widely used in drug discovery. Initially, fluconazole was used as a query, and a broad search strategy identified 5,789 structurally similar compounds [30]. Additionally, 1,683 FDA-approved drugs were evaluated to explore the structural and mechanistic plausibility of the compounds prioritized by ML models against *C. albicans*. Similarity analysis was performed using the Daylight similarity method from ZINC-22, and compounds were considered similar to fluconazole when the structural similarity was greater than or equal to 75% [31].

2.6 MOLECULAR DOCKING

Molecular docking was performed using PyRx 0.8 [32] and AutoDock Vina 1.2.7 [33] for cross-validation of the results. The top three ligands from rigid docking, along with fluconazole, were further evaluated using flexible docking, allowing the flexibility of residues interacting with the reference ligand. All simulations were conducted using an *exhaustiveness* value of 100. Ligands were retrieved from the ZINC20 database in the SDF format [34].

To investigate the potential multi-target activity against *Candida albicans*, six proteins related to fungal growth and cell wall metabolism were screened and identified using their Protein Data Bank (PDB) codes (1EQP, 4QUV, 5TZ1, 5UIV, 4LEB, and 2Y7L) [35]. The canonical antifungal target CYP51 (sterol 14α-demethylase, PDB ID: 5TZ1) was included as a reference target because of its key role in ergosterol biosynthesis [36]. Docking against CYP51 showed that the prioritized ligands displayed higher predicted binding affinities than fluconazole (Supplementary Table S01).

Blind docking identified 1EQP (exo-β-(1,3)-glucanase) as the protein with the lowest binding energy for the reference ligands, leading to its selection for detailed flexible docking and MD simulations. The 1EQP structure

was solved by X-ray diffraction at a resolution of 1.90 Å [37], and redocking was performed using the closely related structure 1EQC [38]. The docking grid was centered at x = 34.08, y = 31.91, z = 57.88, with dimensions of 58.42 × 53.87 × 60.89 Å.

2.6.1 Ligand Preparation

Ligands were initially energy-minimized in PyRx 0.8 using the Universal Force Field (UFF) and the conjugate gradient optimization algorithm, with the following parameters: 200 minimization steps, update at every step, and automatic interruption if the energy difference fell below 0.1 kcal/mol. After minimization, the ligands were converted to PDB format, and the protonation states corresponding to pH 7.4 were computed using the Open Babel software [39]. Subsequently, all ligands were converted to PDBQT format [16].

2.6.2 Protein Preparation

Protein preparation was performed using PDB2PQR (https://server.poissonboltzmann.org/pdb2pqr) [40]. Initially, all water molecules were removed from the structure, which was then processed to calculate the protonation states at pH 7.4, using the AMBER force field. Additional steps included ensuring that newly added atoms were not reconstructed too close to the existing atoms, optimizing the hydrogen-bonding network, and generating an input file for the Adaptive Poisson–Boltzmann Solver (APBS). Subsequently, the Kollman charges were assigned to the protein using AutoDockTools v1.5.7, and the final file was converted to the PDBQT format [41].

2.7 MOLECULAR DYNAMIC SIMULATIONS

The MD simulations were performed to evaluate the structural stability and dynamic behavior of the protein–ligand complexes obtained through molecular docking. Simulations were conducted using GROMACS version 2020.4 [42] and CHARMM36 force field [43,44].

Each complex was solvated in a triclinic box using the TIP3P water model [45]. System neutralization and ionic strength adjustment were achieved by adding Na^+ and Cl^- ions, respectively. Energy minimization was performed prior to equilibration to remove any unfavorable contact. The systems were equilibrated under the NVT and NPT ensembles, maintaining the temperature at 310 K using the V-rescale thermostat [46] and the pressure at 1 bar using the appropriate pressure-coupling method [47]. Following equilibration, production MD simulations of 200 ns were performed using the Leap-Frog integrator [48,49].

Trajectory analyses were performed to assess the stability and flexibility of the systems. The Root Mean Square Deviation (RMSD) was calculated to monitor the structural stability of the complexes over time. The RMSD was calculated based on atomic coordinates extracted from the MD trajectories, according to Equation (1) [50].

$$RMSD = \sqrt{\frac{1}{n}\sum_{i=1}^{N}(x_{i1} - x_{i2})^2 + (y_{i1} - y_{i2})^2 + (z_{i1} - z_{i2})^2} \quad (1)$$

2.8 ADMET PROPERTY ANALYSIS

Following flexible molecular docking, the top-ranked compounds were subjected to *in silico* ADMET analysis using the online platform pkCSM, which predicts pharmacokinetic and toxicity properties of the compounds [51]. The evaluated parameters included absorption (water solubility, Caco-2 permeability, human intestinal absorption, skin permeability, and P-glycoprotein interactions), distribution (volume of distribution, fraction unbound, BBB and CNS permeability), metabolism (CYP450 substrates and inhibitors), excretion (total clearance), and toxicity (AMES mutagenicity, maximum tolerated dose, hERG inhibition, oral rat acute and chronic toxicity, hepatotoxicity, skin sensitization, and aquatic toxicity).

3 RESULTS

3.1 MACHINE LEARNING MODELS

The ML models demonstrated consistent performance in predicting antifungal activity. The Random Forest model showed strong predictive ability, achieving $R^2 = 0.96$ in the training set and 0.89 in the test set, with low error values (MAE = 0.17 and RMSE = 0.23 in training; MAE = 0.26 and RMSE = 0.34 in testing). The Gradient Boosting Regressor also exhibited robust performance, obtaining $R^2 = 0.92$ in training and $R^2 = 0.80$ in testing, with average errors of MAE = 0.24 and RMSE = 0.32 in training, and MAE = 0.31 and RMSE = 0.43 in testing. The Extra Trees Regressor was the best-performing model, achieving $R^2 = 0.97$ in training and 0.90 in testing,

with the lowest error metrics (MAE = 0.14 and RMSE = 0.21 in training; MAE = 0.26 and RMSE = 0.38 in testing). The three regression models showed comparable predictive performances. The Friedman test indicated no statistically significant differences among the models ($\chi^2 = 5.60$, $p = 0.061$). Pairwise comparisons using the Nemenyi post-hoc test also revealed no significant differences (Random forest vs. Extra Trees Regressor: $p = 0.896$; Random forest vs. Gradient Boosting Regressor: $p = 0.065$; Extra Trees Regressor vs. Gradient Boosting Regressor: $p = 0.173$). Figure 2 illustrates the linear regression plots of the developed ML models.

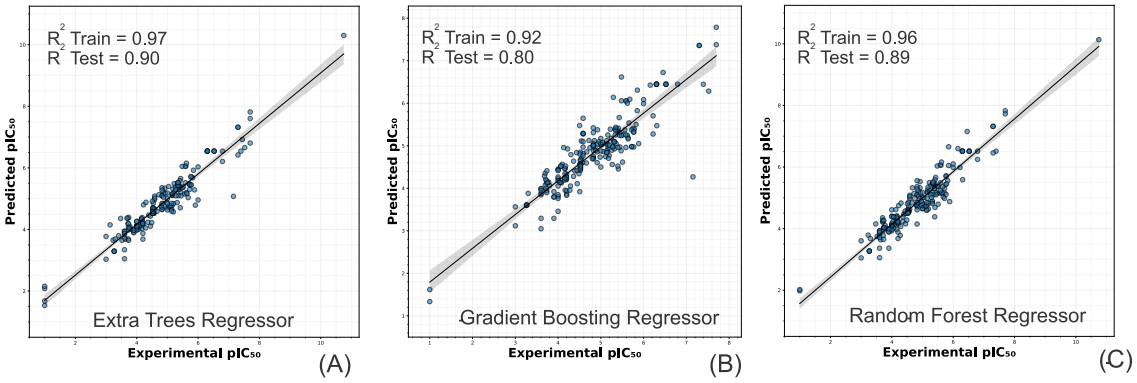


Figure 2. Relationship between the experimental pIC_{50} values and the values predicted by the ML models: (A) Extra Trees Regressor, (B) Gradient Boosting Regressor, and (C) Random Forest Regressor. The lines represent the linear fit between the experimental and predicted values, with the confidence intervals shown in gray. The R^2 for the training and test sets are indicated in each plot.

3.2 IDENTIFICATION OF FLUCONAZOLE ANALOGS AND REPURPOSING OF FDA-APPROVED DRUGS AGAINST *C. ALBICANS*

Table 1 presents the compounds selected from the ZINC-22 database with potential antifungal bioactivity, including fluconazole. The primary selection of candidates was guided by chemometric analyses using ML models. A consensus approach among Random Forest, Extra Trees, and Gradient Boosting models was applied, prioritizing compounds with a predicted pIC_{50} greater than 6.0, a coefficient of variation (CV%) below 2.0, and, for structural analogs, a similarity above 75% [16].

ZINC ID	Extra Trees	Gradient Boosting	Random Forest	Mean	Standard deviation	Coefficient of variation (%)	Similarity with Fluconazole
ZINC000000004009	6.20	6.15	6.20	6.18	0.02	0.35	1.00
ZINC000040844994	6.06	6.16	6.12	6.11	0.04	0.68	0.94
ZINC000040844993	6.06	6.16	6.12	6.11	0.04	0.68	0.94
ZINC000504084521	6.14	6.13	6.12	6.13	0.01	0.18	0.92
ZINC000504084519	6.14	6.13	6.12	6.13	0.01	0.18	0.92
ZINC000038289837	6.14	6.28	6.16	6.19	0.06	0.98	0.90
ZINC000038289836	6.14	6.28	6.16	6.19	0.06	0.98	0.90
ZINC000196183247	6.16	6.30	6.15	6.20	0.07	1.06	0.80
ZINC000196183259	6.16	6.30	6.15	6.20	0.07	1.06	0.80
ZINC000034020906	5.96	6.07	6.01	6.01	0.04	0.72	0.77
ZINC000034020907	5.96	6.07	6.01	6.01	0.04	0.72	0.77
ZINC000103237407	6.05	6.01	6.19	6.08	0.07	1.23	0.77
ZINC000103237409	6.05	6.01	6.19	6.08	0.07	1.23	0.77
ZINC000141515017	6.00	6.23	6.00	6.08	0.11	1.73	0.77
ZINC000141515219	6.00	6.23	6.00	6.08	0.11	1.73	0.77
ZINC000009470585	6.14	5.95	6.11	6.06	0.08	1.36	0.76

ZINC000009470583	6.14	5.95	6.11	6.06	0.08	1.36	0.76
ZINC000299869730	6.12	6.33	6.17	6.21	0.09	1.47	0.75
ZINC000299869729	6.12	6.33	6.17	6.21	0.09	1.47	0.75

Table 1. The table presents the predicted pIC_{50} values for each compound obtained from the Random Forest, ExtraTrees, and Gradient Boosting models, as well as the mean, standard deviation (SD), and CV% of the predictions, which reflect the consistency among the models. The column "Similarity with Fluconazole" indicates the structural similarity of each compound to fluconazole, which was used as an additional criterion for analog selection. Compounds with pIC_{50} greater than 6.0, CV% < 2.0, and similarity > 75% were considered candidates prioritized for further computational for future analyses.

Table 2 presents the FDA-approved drugs that were included as reference compounds in this study. Bioactivity predictions were generated using the Random Forest, ExtraTrees, and Gradient Boosting models, allowing the assessment of result consistency in comparison with established antifungal agents.

Name	Random Forest	Gradient Boosting	Extra Trees	Mean	Standard deviation	Coefficient of variation (%)
Miconazole	6.06	6.06	6.05	6.06	0.00	0.06
CID 78318119	6.13	6.13	6.11	6.12	0.01	0.16
Rezafungin	6.13	6.13	6.11	6.12	0.01	0.16
Caspofungin	7.32	7.36	7.32	7.33	0.02	0.25
Fluconazole	6.20	6.15	6.20	6.18	0.02	0.35
Amphotericin B	6.51	6.45	6.54	6.50	0.04	0.63
Ketoconazole	6.37	6.26	6.38	6.34	0.05	0.84
Everolimus	6.01	6.06	5.93	6.00	0.05	0.86
Sirolimus	6.21	6.09	6.21	6.17	0.05	0.88
Flucytosine	6.27	6.12	6.27	6.22	0.07	1.12
Cefotaxime	6.54	6.37	6.59	6.50	0.09	1.43
Meropenem	6.28	6.00	6.23	6.17	0.12	1.95

Table 2. The mean pIC_{50} values, SD, and CV were calculated from the predictions of the three models, providing a comparative evaluation of the predicted bioactivity of FDA-approved drugs.

3.3 MOLECULAR DOCKING

For protocol validation, the redocking of the co-crystallized ligand into the protein structure 1EQC was performed, resulting in an RMSD of 0.454 Å, which confirmed the reliability of the docking protocol [52]. The reference drug fluconazole established key interactions with essential active site residues, including GLU27, ASP145, ASN146, PHE144, PHE258, HIS135, and GLU192.

The predicted binding energies of the screened compounds, calculated using rigid docking with AutoDock Vina 1.2.7, are presented in Figure 3, and the consensus docking results from AutoDock Vina 1.2.7 and PyRx 0.8 are summarized in Table S2 of the Supplementary Material.

Flexible docking further supports these observations. Fluconazole showed binding energies of –8.63 kcal/mol (rigid) and –8.87 kcal/mol (flexible), serving as a reference for comparative assessment. Notably, ZINC000299869730 exhibited stronger predicted binding affinities of –9.11 kcal/mol (rigid) and –10.27 kcal/mol (flexible), suggesting a potentially higher *in silico* affinity than that of fluconazole. Similarly, ZINC000299869729 displayed binding energies of –9.40 kcal/mol (rigid) and –9.61 kcal/mol (flexible), reinforcing its potential as a candidate.

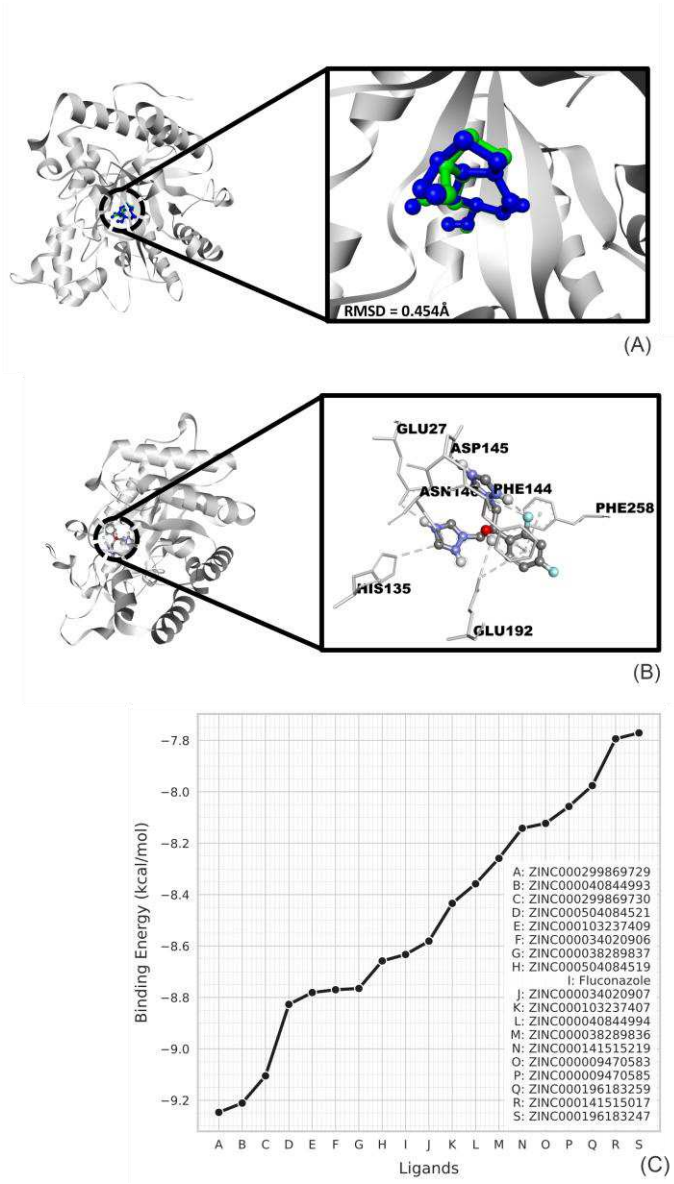


Figure 3. Results of the molecular docking study. (A) Redocking of the co-crystallized ligand in protein 1EQC, yielding an RMSD of 0.454 Å. (B) Interactions of the reference drug fluconazole with active site residues (GLU27, ASP145, ASN146, PHE144, PHE258, HIS135, and GLU192). (C) Binding energies (kcal/mol) obtained through rigid docking using AutoDock Vina 1.2.7, considering only the lowest energy pose for each ligand.

3.4 MOLECULAR DYNAMIC SIMULATIONS

Figure 4 presents the RMSD profiles obtained from the 200 ns MD simulations for all evaluated systems: the apo protein (black), fluconazole–protein complex (red), ZINC000299869729 complex (green), and ZINC000299869730 complex (blue). RMSD analysis was used to assess the structural stability and conformational behavior of the systems over time.

The apo protein exhibited the most stable profile, with RMSD values ranging from 0.10 to 0.18 nm, rapidly equilibrating, and remaining close to its initial conformation throughout the simulation period. After approximately 100 ns, the system exhibited reduced deviations and minimal conformational fluctuations, indicating a high degree of structural stability. The fluconazole–protein complex displayed similar behavior, with RMSD values between 0.15 and 0.20 nm, suggesting that ligand binding did not induce significant structural changes.

In contrast, the ZINC000299869729 complex initially showed stable behavior but exhibited increased deviations after approximately 150 ns, reaching RMSD values between 0.25 and 0.30 nm, indicating greater conformational variability. The ZINC000299869730 complex stabilized rapidly after approximately 60 ns, maintaining RMSD

values of approximately 0.20 nm during the final phase of the simulation, which is consistent with previously reported correlations between RMSD stabilization and system stability [53].

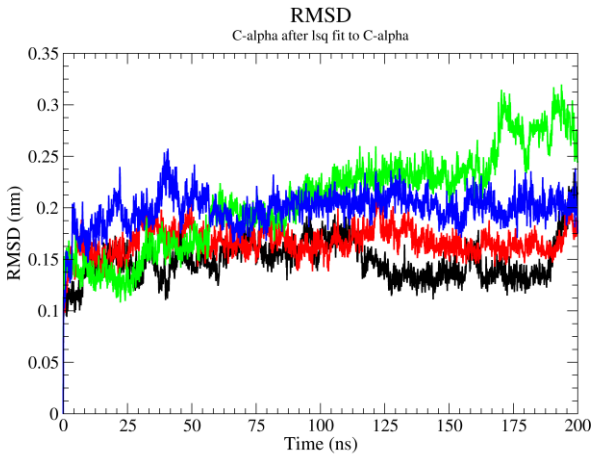


Figure 4. RMSD values for MD studies associated with the constructed systems 1eqp clean (Black), complex formed with fluconazole (Red), ZINC000299869729 (Green), and ZINC000299869730 (Blue).

The hydrogen bond occupancy analysis is shown in figure 5, summarizing the interactions formed between the ligands and active site residues throughout the 200 ns simulations. Fluconazole exhibited predominantly low hydrogen bond occupancy values (approximately 5–20%), suggesting that its binding is largely stabilized by non-polar interactions. In contrast, ZINC000299869729 formed a greater number of hydrogen bonds with higher occupancies, particularly involving residues Glu27, Glu292, and Leu304, which reached approximately 50%. ZINC000299869730 displayed fewer hydrogen bond interactions, with a maximum occupancy of approximately 12.3%, and mainly involved the residue Tyr153.

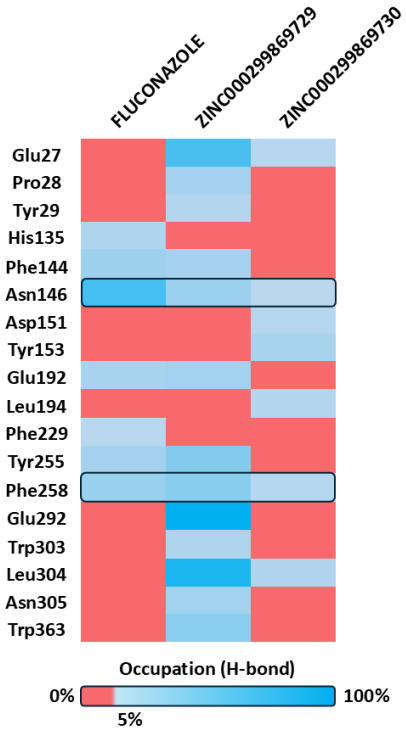


Figure 5. Hydrogen bonds between ligands are present in the interaction cavity with amino acid residues.

Notably, all three complexes exhibited recurrent interactions with residues Asn146 and Phe258, supporting the docking predictions that the ligands occupy similar regions within the binding sites.

3.5 ADMET PROPERTIES

The ADMET profiles of compounds ZINC000299869730 and ZINC000299869729 exhibited ADMET profiles comparable to those of fluconazole. Both compounds showed good predicted human intestinal absorption (≈81.6%), although they had lower aqueous solubility and Caco-2 permeability than the reference drug. Distribution analysis indicated a low volume of distribution, high plasma protein binding, and low permeability across the blood–brain barrier and central nervous system.

Regarding metabolism, both candidates were predicted to be CYP3A4 substrates, with no relevant inhibitory effects on the major CYP450 isoforms, suggesting a lower risk of drug–drug interactions than that of fluconazole. The compounds also exhibited reduced total clearance. Toxicity predictions revealed a profile comparable to that of the reference drug, including predicted AMES mutagenicity and hepatotoxicity, absence of hERG-associated cardiotoxicity, and low skin-sensitization potential. The complete results are presented in Table 3.

Category	Property	Fluconazole	ZINC000299869730	ZINC000299869729	Unit / Type
Absorption	Water solubility	−3.023	−3.982	−3.982	log mol/L
	Caco-2 permeability	0.387	−0.154	−0.154	log Papp (10^{-6} cm/s)
	Human intestinal absorption	85.48	81.59	81.59	% absorbed
	Skin permeability	−3.296	−2.834	−2.834	log Kp
	P-glycoprotein substrate	Yes	Yes	Yes	Yes / No
	P-glycoprotein I inhibitor	No	No	No	Yes / No
	P-glycoprotein II inhibitor	No	No	No	Yes / No
Distribution	Volume of distribution (human)	−1.326	−1.634	−1.634	log L/kg
	Fraction unbound (human)	0.373	0.291	0.291	—
	Blood-brain barrier permeability	−1.075	−1.604	−1.604	log BB
	CNS permeability	−3.405	−3.533	−3.533	log PS
Metabolism	CYP2D6 substrate	No	No	No	Yes / No
	CYP3A4 substrate	No	Yes	Yes	Yes / No
	CYP1A2 inhibitor	Yes	No	No	Yes / No
	CYP2C19 inhibitor	No	No	No	Yes / No
	CYP2C9 inhibitor	No	No	No	Yes / No
	CYP2D6 inhibitor	No	No	No	Yes / No

	CYP3A4 inhibitor	No	No	No	Yes / No
Excretion	Total clearance	0.28	0.053	0.053	log mL/min/kg
Toxicity	AMES toxicity	Yes	Yes	Yes	Yes / No
	Maximum tolerated dose (human)	0.884	0.884	0.884	log mg/kg/day
	hERG I inhibitor	No	No	No	Yes / No
	hERG II inhibitor	No	No	No	Yes / No
	Oral rat acute toxicity (LD_{50})	2.451	2.391	2.391	mol/kg
	Oral rat chronic toxicity (LOAEL)	1.455	1.758	1.758	log mg/kg_bw/day
	Hepatotoxicity	Yes	Yes	Yes	Yes / No
	Skin sensitization	No	No	No	Yes / No

Table 3. Predicted ADMET parameters (absorption, distribution, metabolism, excretion, and toxicity) of fluconazole and the selected compounds from flexible docking (ZINC000299869730 and ZINC000299869729).

4 DISCUSSION

Fungal infections caused by *Candida albicans* represent an increasing global health challenge, particularly due to the rising resistance to fluconazole, which significantly limits available therapeutic options [1]. In this context, the identification of novel antifungal agents has become a priority, and computational approaches such as QSAR modeling combined with ML have emerged as promising tools to accelerate the discovery of effective candidates. In the present study, a QSAR/ML-based workflow demonstrated high predictive performance, enabling the efficient identification and prioritization of compounds with potential antifungal activity. The use of Morgan fingerprints (ECFP4) as molecular descriptors, combined with variance filtering, contributed to reducing noise and dimensionality while preserving relevant structural features, thereby improving model performance. The consistency of predictions across different algorithms further supports the robustness of the approach and its ability to capture structural patterns associated with antifungal activity.

Indirect validation of the models was observed through the coherent prediction of established antifungal agents, such as fluconazole, amphotericin B, and caspofungin, which exhibited high pIC_{50} values and low variability across models [54]. However, the identification of non-antifungal compounds, including β-lactam antibiotics and immunosuppressants, highlights inherent limitations of QSAR/ML models, particularly the occurrence of false positives. This may be partially explained by the fact that such agents can indirectly enhance fungal virulence: β-lactam antibiotics may promote fungal overgrowth through competitive disruption of the host microbiota, reducing bacterial competition [55], whereas immunosuppressants can weaken host immune defenses, thereby facilitating fungal proliferation and pathogenicity [56]. These findings emphasize the need for critical pharmacological interpretation and experimental validation, as high statistical performance does not necessarily guarantee biological relevance.

Among the prioritized compounds, ZINC000299869730 emerged as the most promising candidate. Molecular docking studies against exo-β-(1,3)-glucanase revealed a higher binding affinity compared to fluconazole, suggesting an enhanced potential for target interaction. Detailed analysis of the active site showed that key catalytic residues, such as Glu192 and Glu292, play essential roles in the enzymatic mechanism, acting as acid/base and nucleophile, respectively. The residue Glu27 contributes to substrate recognition through hydrogen bonding, while aromatic residues such as Phe144 and Phe258 form an “aromatic gate” that guides and stabilizes the ligand within the catalytic site [37].

Functionally, exo-1,3-β-glucanase plays a critical role in fungal cell wall remodeling, participating in both hydrolysis and reorganization of β-glucans. Inhibition of this enzyme compromises cell wall structural integrity,

leading to reduced rigidity, increased susceptibility to environmental stress, and diminished capacity for hyphal and biofilm formation, factors directly associated with virulence and antifungal resistance [37].

While docking results provide an initial estimate of binding affinity, molecular dynamics simulations offer a more robust assessment of complex stability. The compound ZINC000299869730 exhibited consistent structural stability throughout the simulation, with localized fluctuations compatible with adaptive conformational adjustments, without compromising the overall protein integrity. In contrast, ZINC000299869729 displayed greater conformational flexibility, suggesting lower structural complementarity. These results indicate that the persistence of interactions over time is a more reliable indicator of inhibitory potential than docking scores alone.

Additionally, docking studies against CYP51, a classical target of azole antifungals, revealed binding affinities higher than those of fluconazole for the selected compounds, suggesting a possible multitarget profile. Although molecular dynamics simulations were not performed for this target, the observed interactions indicate biological relevance and warrant further investigation.

ADMET predictions indicated that the compounds exhibit overall favorable pharmacokinetic properties comparable to fluconazole. High intestinal absorption, combined with low central nervous system permeability, suggests suitability for systemic use with a reduced risk of central adverse effects. Furthermore, the lack of significant inhibition of major cytochrome P450 isoforms indicates a low potential for drug–drug interactions.

However, predicted toxicity signals, particularly mutagenicity (AMES) and hepatotoxicity, represent important limitations. Positive AMES test predictions suggest potential genotoxicity, as outlined in the guidelines of the International Council for Harmonisation of Technical Requirements for Pharmaceuticals for Human Use (ICH S2(R1)), which recommend further *in vitro* and *in vivo* investigations to confirm mutagenic risk [57].

5 CONCLUSION

ZINC000299869730 and ZINC000299869729 were identified as computationally prioritized fluconazole analogs, exhibiting higher predicted binding affinities for both exo-β-(1,3)-glucanase (PDB: 1EQP) and CYP51 (PDB: 5TZ1), suggesting a potential multitarget binding profile. MD simulations indicated that ZINC000299869730 combined global structural stability with localized fluctuations consistent with adaptive rearrangements at the active site, whereas ZINC000299869729 displayed greater conformational flexibility while maintaining the relevant binding interactions. Both compounds demonstrated favorable ADMET profiles, including good intestinal absorption, low risk of drug–drug interactions, limited blood–brain barrier permeability, and absence of predicted cardiotoxicity.

Although these computational results suggest significant antifungal potential, the main limitation of this study is the absence of experimental validation, which is essential for confirming the predicted activity and safety. Future work will include MD simulations with the canonical target CYP51, chemical optimization of the identified compounds to further enhance their ADMET properties, laboratory synthesis, followed by *in vitro* antifungal testing, establishing a clear path to validate and advance these candidates.

Overall, this study demonstrates the utility of an integrated ML–guided computational workflow to efficiently accelerate the screening and prioritization of antifungal candidates, providing a robust foundation for continued experimental studies and rational drug development.

ACKNOWLEDGEMENTS: Emmanuel Silva Marinho acknowledges financial support from the Funding Agency of Ceará- FUNCAP (Grant#: FPD-0213-00369.01.00/23) e National Council for Scientific and Technological Development CNPQ-PQ [Grant#: 309349/2025-7].

6 REFERENCES

[1] Li Y, Qiao Y, Ma Y, Xue P, Ding C. AI in fungal drug development: opportunities, challenges, and future outlook. Front Cell Infect Microbiol 2025;15. https://doi.org/10.3389/fcimb.2025.1610743.

[2] Yiu B, Robbins N, Cowen LE. Interdisciplinary approaches for the discovery of novel antifungals. Trends in Molecular Medicine 2024;30:723–35. https://doi.org/10.1016/j.molmed.2024.04.018.

[3] Cornely OA, Sprute R, Bassetti M, Chen SC-A, Groll AH, Kurzai O, et al. Global guideline for the diagnosis and management of candidiasis: an initiative of the ECMM in cooperation with ISHAM and ASM. The Lancet Infectious Diseases 2025;25:e280–93. https://doi.org/10.1016/S1473-3099(24)00749-7.

[4] Jp L, Ms L. Pathogenesis and virulence of Candida albicans. Virulence 2022;13. https://doi.org/10.1080/21505594.2021.2019950.

[5] Sobel JD. Resistance to Fluconazole of Candida albicans in Vaginal Isolates: a 10-Year Study in a Clinical Referral Center. Antimicrobial Agents and Chemotherapy 2023;67:e00181-23. https://doi.org/10.1128/aac.00181-23.
[6] Nguyen MD, Ren P. Trends in Antifungal Resistance Among Candida Species: An Eight-Year Retrospective Study in the Galveston-Houston Gulf Coast Region. J Fungi (Basel) 2025;11:232. https://doi.org/10.3390/jof11030232.
[7] Lamoth F. Novel Therapeutic Approaches to Invasive Candidiasis: Considerations for the Clinician. IDR 2023;16:1087–97. https://doi.org/10.2147/IDR.S375625.
[8] de Almeida TF, Cunha-Junior EF, Wanderley JLM, Pacheco J da S, Pinto-da-Silva LH, Andrade-Neto VV, et al. Editorial: Strategies in the drug discovery and development for leishmaniasis: immunomodulators, natural products, synthetic compounds, and drug repositioning. Front Cell Infect Microbiol 2024;14. https://doi.org/10.3389/fcimb.2024.1384244.
[9] Sarkar C, Das B, Rawat VS, Wahlang JB, Nongpiur A, Tiewsoh I, et al. Artificial Intelligence and Machine Learning Technology Driven Modern Drug Discovery and Development. Int J Mol Sci 2023;24:2026. https://doi.org/10.3390/ijms24032026.
[10] Theodosiou AA, Read RC. Artificial intelligence, machine learning and deep learning: Potential resources for the infection clinician. J Infect 2023;87:287–94. https://doi.org/10.1016/j.jinf.2023.07.006.
[11] Erickson BJ. Basic Artificial Intelligence Techniques: Machine Learning and Deep Learning. Radiol Clin North Am 2021;59:933–40. https://doi.org/10.1016/j.rcl.2021.06.004.
[12] Salimi A, Lim JH, Jang JH, Lee JY. The use of machine learning modeling, virtual screening, molecular docking, and molecular dynamics simulations to identify potential VEGFR2 kinase inhibitors. Sci Rep 2022;12:18825. https://doi.org/10.1038/s41598-022-22992-6.
[13] Zdrazil B, Felix E, Hunter F, Manners EJ, Blackshaw J, Corbett S, et al. The ChEMBL Database in 2023: a drug discovery platform spanning multiple bioactivity data types and time periods. Nucleic Acids Res 2024;52:D1180–92. https://doi.org/10.1093/nar/gkad1004.
[14] Padalino G, Coghlan A, Pagliuca G, Forde-Thomas JE, Berriman M, Hoffmann KF. Using ChEMBL to Complement Schistosome Drug Discovery. Pharmaceutics 2023;15:1359. https://doi.org/10.3390/pharmaceutics15051359.
[15] Target: Candida albicans (CHEMBL366) n.d. https://www.ebi.ac.uk/explore/target/CHEMBL366 (accessed July 13, 2025).
[16] Cobre A de F, Ara A, Alves AC, Maia Neto M, Fachi MM, Beca LS dos AB, et al. Identifying 124 new *anti*-HIV drug candidates in a 37 billion-compound database: An integrated approach of machine learning (QSAR), molecular docking, and molecular dynamics simulation. Chemometrics and Intelligent Laboratory Systems 2024;250:105145. https://doi.org/10.1016/j.chemolab.2024.105145.
[17] Kunzelmann M, Wittmann A, Nold V, Presser B, Schreiber J, Gehrig T, et al. Functional design of experiment for potency assay optimization and in-silico simulation. J Pharm Biomed Anal 2023;234:115584. https://doi.org/10.1016/j.jpba.2023.115584.
[18] Maattallaoui I, Sakho M, Maatallaoui A, Catalán EB, Aouad NE. Development of QSAR Models and Web Applications for Predicting hDHFR Inhibitor Bioactivity Using Machine Learning. Molecules 2025;30:4618. https://doi.org/10.3390/molecules30234618.
[19] Yang J, Cai Y, Zhao K, Xie H, Chen X. Concepts and applications of chemical fingerprint for hit and lead screening. Drug Discovery Today 2022;27:103356. https://doi.org/10.1016/j.drudis.2022.103356.
[20] Dolciami D, Villasclaras-Fernandez E, Kannas C, Meniconi M, Al-Lazikani B, Antolin AA. canSAR chemistry registration and standardization pipeline. J Cheminform 2022;14:28. https://doi.org/10.1186/s13321-022-00606-7.
[21] Li J, Othman MS, Chen H, Yusuf LM. Optimizing IoT intrusion detection system: feature selection versus feature extraction in machine learning. J Big Data 2024;11:36. https://doi.org/10.1186/s40537-024-00892-y.
[22] Xu S, Vaughan J, Chen J, Sudjianto A, Nair V. Supervised Linear Dimension-Reduction Methods: Review, Extensions, and Comparisons 2021. https://doi.org/10.48550/arXiv.2109.04244.
[23] Yoo C, Shahlaei M. The applications of PCA in QSAR studies: A case study on CCR5 antagonists. Chem Biol Drug Des 2018;91:137–52. https://doi.org/10.1111/cbdd.13064.
[24] Sharma O, Ghantasala GSP, Ioannou I, Vassiliou V. Advancing pneumonia virus drug discovery with virtual screening: A cutting-edge fast and resource efficient machine learning framework for predictive analysis. Informatics in Medicine Unlocked 2024;47:101471. https://doi.org/10.1016/j.imu.2024.101471.
[25] Capecchi A, Awale M, Probst D, Reymond J-L. PubChem and ChEMBL beyond Lipinski. Mol Inform 2019;38:e1900016. https://doi.org/10.1002/minf.201900016.

[26] Pitakbut T, Munkert J, Xi W, Wei Y, Fuhrmann G. A dataset for machine learning-based QSAR models establishment to screen beta-lactamase inhibitors using the FARM -BIOMOL chemical library. BMC Res Notes 2025;18:91. https://doi.org/10.1186/s13104-025-07159-6.
[27] Feurer M, Hutter F. Hyperparameter Optimization. In: Hutter F, Kotthoff L, Vanschoren J, editors. Automated Machine Learning: Methods, Systems, Challenges, Cham: Springer International Publishing; 2019, p. 3–33. https://doi.org/10.1007/978-3-030-05318-5_1.
[28] Kamble VH, Dale MP. Chapter 1 - Machine learning approach for longitudinal face recognition of children. In: Sarangi PP, Panda M, Mishra S, Mishra BSP, Majhi B, editors. Machine Learning for Biometrics, Academic Press; 2022, p. 1–27. https://doi.org/10.1016/B978-0-323-85209-8.00011-0.
[29] Lee J, Hong H, Song JM, Yeom E. Neural network ensemble model for prediction of erythrocyte sedimentation rate (ESR) using partial least squares regression. Sci Rep 2022;12:19618. https://doi.org/10.1038/s41598-022-23174-0.
[30] Tingle BI, Tang KG, Castanon M, Gutierrez JJ, Khurelbaatar M, Dandarchuluun C, et al. ZINC-22—A Free Multi-Billion-Scale Database of Tangible Compounds for Ligand Discovery. J Chem Inf Model 2023;63:1166–76. https://doi.org/10.1021/acs.jcim.2c01253.
[31] Franco P, Porta N, Holliday JD, Willett P. The use of 2D fingerprint methods to support the assessment of structural similarity in orphan drug legislation. Journal of Cheminformatics 2014;6:5. https://doi.org/10.1186/1758-2946-6-5.
[32] Dallakyan S, Olson AJ. Small-Molecule Library Screening by Docking with PyRx. In: Hempel JE, Williams CH, Hong CC, editors. Chemical Biology: Methods and Protocols, New York, NY: Springer; 2015, p. 243–50. https://doi.org/10.1007/978-1-4939-2269-7_19.
[33] Eberhardt J, Santos-Martins D, Tillack AF, Forli S. AutoDock Vina 1.2.0: New Docking Methods, Expanded Force Field, and Python Bindings. J Chem Inf Model 2021;61:3891–8. https://doi.org/10.1021/acs.jcim.1c00203.
[34] Irwin JJ, Tang KG, Young J, Dandarchuluun C, Wong BR, Khurelbaatar M, et al. ZINC20—A Free Ultralarge-Scale Chemical Database for Ligand Discovery. J Chem Inf Model 2020;60:6065–73. https://doi.org/10.1021/acs.jcim.0c00675.
[35] Manzano JAH, Brogi S, Calderone V, Macabeo APG, Austriaco N. Globospiramine Exhibits Inhibitory and Fungicidal Effects against Candida albicans via Apoptotic Mechanisms. Biomolecules 2024;14:610. https://doi.org/10.3390/biom14060610.
[36] Hargrove TY, Friggeri L, Wawrzak Z, Qi A, Hoekstra WJ, Schotzinger RJ, et al. Structural analyses of Candida albicans sterol 14α-demethylase complexed with azole drugs address the molecular basis of azole-mediated inhibition of fungal sterol biosynthesis. J Biol Chem 2017;292:6728–43. https://doi.org/10.1074/jbc.M117.778308.
[37] Cutfield JF, Sullivan PA, Cutfield SM. Minor structural consequences of alternative CUG codon usage (Ser for Leu) in Candida albicans exoglucanase. Protein Eng 2000;13:735–8. https://doi.org/10.1093/protein/13.10.735.
[38] Cutfield SM, Davies GJ, Murshudov G, Anderson BF, Moody PCE, Sullivan PA, et al. The structure of the exo-β-(1,3)-glucanase from *Candida albicans* in native and bound forms: relationship between a pocket and groove in family 5 glycosyl hydrolases1. Journal of Molecular Biology 1999;294:771–83. https://doi.org/10.1006/jmbi.1999.3287.
[39] O'Boyle NM, Banck M, James CA, Morley C, Vandermeersch T, Hutchison GR. Open Babel: An open chemical toolbox. J Cheminform 2011;3:33. https://doi.org/10.1186/1758-2946-3-33.
[40] Dolinsky TJ, Czodrowski P, Li H, Nielsen JE, Jensen JH, Klebe G, et al. PDB2PQR: expanding and upgrading automated preparation of biomolecular structures for molecular simulations. Nucleic Acids Res 2007;35:W522–5. https://doi.org/10.1093/nar/gkm276.
[41] Sastry GM, Adzhigirey M, Day T, Annabhimoju R, Sherman W. Protein and ligand preparation: parameters, protocols, and influence on virtual screening enrichments. J Comput Aided Mol Des 2013;27:221–34. https://doi.org/10.1007/s10822-013-9644-8.
[42] De Oliveira VM, Da Rocha MN, Roberto CHA, Lucio FNM, Marinho MM, Marinho ES, et al. Insights of structure-based virtual screening and MPO-based SAR analysis of berberine-benzimidazole derivatives against Parkinson disease. Journal of Molecular Structure 2024;1302:137453. https://doi.org/10.1016/j.molstruc.2023.137453.
[43] Huang J, Rauscher S, Nawrocki G, Ran T, Feig M, De Groot BL, et al. CHARMM36m: An improved force field for folded and intrinsically disordered proteins. Nature Methods 2017;14:71–3. https://doi.org/10.1038/nmeth.4067.
[44] Yu Y, Krämer A, Venable RM, Simmonett AC, Mackerell AD, Klauda JB, et al. Semi-automated Optimization of the CHARMM36 Lipid Force Field to Include Explicit Treatment of Long-Range

Dispersion. Journal of Chemical Theory and Computation 2021;17:1562–80. https://doi.org/10.1021/acs.jctc.0c01326.
[45] Boonstra S, Onck PR, Van Der Giessen E. CHARMM TIP3P Water Model Suppresses Peptide Folding by Solvating the Unfolded State. Journal of Physical Chemistry B 2016;120:3692–8. https://doi.org/10.1021/acs.jpcb.6b01316.
[46] Nagasundaram N, Wilson Alphonse CR, Samuel Gnana PV, Rajaretinam RK. Molecular Dynamics Validation of Crizotinib Resistance to ALK Mutations (L1196M and G1269A) and Identification of Specific Inhibitors. Journal of Cellular Biochemistry 2017;118:3462–71. https://doi.org/10.1002/jcb.26004.
[47] Verma R, Pradhan D, Nayek A, Singh H, Jain AK, Khan LA. Target-based drug repurposing against *Candida albicans* —A computational modeling, docking, and molecular dynamic simulations study. J of Cellular Biochemistry 2022;123:289–305. https://doi.org/10.1002/jcb.30163.
[48] Rabaan AA, Alfouzan WA, Garout M, Halwani MA, Alotaibi N, Alfaresi M, et al. Antifungal drug discovery for targeting *Candida albicans* morphogenesis through structural dynamics study. Journal of Biomolecular Structure and Dynamics 2025;43:6252–68. https://doi.org/10.1080/07391102.2024.2332507.
[49] Pereira AMG, De Oliveira VM, Da Rocha MN, Roberto CHA, Cajazeiras FFM, Guedes JM, et al. Structure and Ligand Based Virtual Screening and MPO Topological Analysis of Triazolo Thiadiazepine-fused Coumarin Derivatives as Anti-Parkinson Drug Candidates. Mol Biotechnol 2025;67:2339–56. https://doi.org/10.1007/s12033-024-01200-y.
[50] da Fonseca AM, Caluaco BJ, Madureira JMC, Cabongo SQ, Gaieta EM, Djata F, et al. Screening of potential inhibitors targeting the main protease structure of SARS-CoV-2 via molecular docking, and approach with molecular dynamics, RMSD, RMSF, H-bond, SASA and MMGBSA. Molecular Biotechnology 2023:1–15.
[51] Pires DEV, Blundell TL, Ascher DB. pkCSM: Predicting Small-Molecule Pharmacokinetic and Toxicity Properties Using Graph-Based Signatures. J Med Chem 2015;58:4066–72. https://doi.org/10.1021/acs.jmedchem.5b00104.
[52] Nivatya HK, Singh A, Kumar N, Sonam, Sharma L, Singh V, et al. Assessing molecular docking tools: understanding drug discovery and design. Future Journal of Pharmaceutical Sciences 2025;11:1–31. https://doi.org/10.1186/s43094-025-00862-y.
[53] Guterres H, Im W. Improving Protein-Ligand Docking Results with High-Throughput Molecular Dynamics Simulations. J Chem Inf Model 2020;60:2189–98. https://doi.org/10.1021/acs.jcim.0c00057.
[54] Patterson TF, Thompson GR, Denning DW, Fishman JA, Hadley S, Herbrecht R, et al. Practice Guidelines for the Diagnosis and Management of Aspergillosis: 2016 Update by the Infectious Diseases Society of America. Clin Infect Dis 2016;63:e1–60. https://doi.org/10.1093/cid/ciw326.
[55] Delavy M, Burdet C, Sertour N, Devente S, Docquier J-D, Grall N, et al. A Clinical Study Provides the First Direct Evidence That Interindividual Variations in Fecal β-Lactamase Activity Affect the Gut Mycobiota Dynamics in Response to β-Lactam Antibiotics. mBio 2022;13:e0288022. https://doi.org/10.1128/mbio.02880-22.
[56] Klawitter J, Nashan B, Christians U. Everolimus and Sirolimus in Transplantation-Related but Different. Expert Opin Drug Saf 2015;14:1055–70. https://doi.org/10.1517/14740338.2015.1040388.
[57] Research C for DE and. S2(R1) Genotoxicity Testing and Data Interpretation for Pharmaceuticals Intended for Human Use 2020. https://www.fda.gov/regulatory-information/search-fda-guidance-documents/s2r1-genotoxicity-testing-and-data-interpretation-pharmaceuticals-intended-human-use (accessed March 22, 2026).

Supplementary Files

This is a list of supplementary files associated with this preprint. Click to download.

- SupplementarymaterialFluconazole.docx